PHYSICAL REVIEW A **81**, 042327 (2010)

Ground-state entanglement in a system with many-body interactions

Xinhua Peng,[1,2,*] Jingfu Zhang,[2] Jiangfeng Du,[1] and Dieter Suter[2,†]
[1]*Hefei National Laboratory for Physical Sciences at Microscale and Department of Modern Physics, University of Science and Technology of China, Hefei, Anhui 230026, People's Republic of China*
[2]*Fakultät Physik, Technische Universität Dortmund, D-44221 Dortmund, Germany*

(Received 7 December 2009; published 27 April 2010)

Entanglement refers to the inability of many-body quantum mechanical systems to be separated into independent subsystems. This has been well investigated in systems consisting of two entangled subsystems. In larger systems, more complex types of entanglement exist. In a system consisting of three subsystems (e.g., qubits), it is possible that all three subsystems are entangled with each other in a way that cannot be reduced to bipartite entanglement, and it is known that two different, inequivalent forms of tripartite entanglement exist such as the GHZ and *W* states (GHZ denotes "Greenberger-Horne-Zeilinger"). Here, we investigate a particularly interesting system with competing one-, two-, and three-body interactions. Its ground state can be a product state, a GHZ state, or a *W* state, depending on the type and strength of the spin-spin couplings. By varying an external control parameter, the system can be made to undergo quantum transitions between the various ground-state-entanglement phases. We implement the system in an NMR quantum simulator and use adiabatic evolution of the effective Hamiltonian to drive the system through the quantum transitions. In the experimental and numerical simulations, we check the suitability of different observables for making the quantum transitions visible and for characterizing the different phases.

DOI: 10.1103/PhysRevA.81.042327 PACS number(s): 03.67.Mn, 03.65.Ud

I. INTRODUCTION

The ground state of a quantum mechanical system usually depends on different parameters, such as the strength of external fields or internal interactions. For certain values of these parameters, the nature of the ground state changes discontinuously; these changes are referred to as quantum phase transitions (QPTs). In analogy to classical (mostly thermally driven) phase transitions, they are induced by a control parameter and may be associated with an order parameter [1]. Examples of QPTs include ferromagnetic to antiferromagnetic phase transitions in quantum magnets [1], the change of conductivity in the Mott insulator to superfluid transition [2,3], and the quantum Hall effect [4].

The entanglement of ground states is one of the aspects that distinguishes quantum phase transitions from their classical analogs. The study of this type of QPTs showed interesting connections between condensed-matter physics and quantum information. A number of authors have analyzed the change of entanglement in systems undergoing QPTs, including the Heisenberg model [5–10] and the Hubbard model [11–13], and found interesting scaling behaviors in the vicinity of quantum critical points.

Many of the relevant features, like the transition from a simple product state to a strongly entangled state, occur over a wide range of parameters and persist for infinite systems as well as for systems with as few as two spins [14–18]. We have experimentally observed such an entangling transition of a two-qubit Heisenberg spin chain by varying the external magnetic field [19]. The transition can be monitored either by performing complete quantum state tomography for each phase or, more efficiently, by suitably coupling the system to an additional probe qubit and performing a suitable measurement on that [20].

In the two-qubit system that we discussed in these earlier papers, only one type of entanglement exists. As we move to larger systems, we obtain a qualitatively different behavior: The system can now exhibit different types of entanglement—either simultaneously or in different phases. As an example, consider a three-qubit system: in this case, two qualitatively different types of tripartite entanglement can be distinguished [21]. The two types of tripartite entanglement (GHZ type, where GHZ denotes "Greenberger-Horne-Zeilinger," and *W* type) differ in important ways and cannot be transformed into each other by local transformations. In particular, if a system is in a pure GHZ state and any one of the three qubits is lost or measured on the computational basis $\{|0\rangle, |1\rangle\}$, the subsystem consisting of the two remaining qubits is definitely in a product state. In contrast, if the system is initially in a *W* state, the bipartite entanglement can be observed after a measurement on one of the qubits. In the case of the GHZ state, we refer to the entanglement as purely three-way entanglement, whereas the *W* state has only pairwise entanglement [21]. Depending on the system parameters, the ground state of the system can be a product state or any of these entangled states. In parameter space, these different ground states form a phase diagram with different entanglement phases. Compared to a two-qubit system, a three-qubit system therefore has richer physics and requires more specific measures for characterizing the different possible ground-state properties.

In this article, we consider spin systems with Ising-type two-body interactions $I_z^i I_z^{i+1}$ and three-body interactions $I_z^i I_z^{i+1} I_z^{i+2}$. This system shows all the characteristics discussed above: depending on the control parameters, the ground state is either a product state, a GHZ state, or a *W* state. More interesting is that the three-body interactions induce a novel quantum transition that does not occur in systems having only two-body interactions [22–25]. We have demonstrated

---

[*] xhpeng@ustc.edu.cn
[†] Dieter.Suter@tu-dortmund.de

©2010 The American Physical Society

the feature in a proof-of-principle experiment with a three-spin system, where both kinds of quantum transitions are successfully detected by entanglement witnesses [26]. Here we investigate such a system in detail and illustrate the connection between the transition and ground-state entanglement.

We implement this system experimentally in an NMR quantum simulator. Using a suitable adiabatic time-dependence of the control parameter in the Hamiltonian, we transfer the system from a product state to one of the entangled ground states. We verify the nature of the state (and its entanglement) by performing a complete quantum state tomography of the final state. In addition to these experimental investigations, we also perform numerical simulations of larger spin chains and present different measures of entanglement that appear more suitable for characterizing these systems than the simple two-qubit concurrence.

II. SYSTEM AND PHASE DIAGRAM OF THE GROUND STATE

We consider the simplest possible case involving both the two- and three-body interactions:

$$\mathcal{H} = \omega_z \sum_{i=1}^{3} I_z^i + \omega_x \sum_{i=1}^{3} I_x^i + 2J_2 \sum_{i=1}^{3} I_z^i I_z^{i+1} + 4J_3 I_z^1 I_z^2 I_z^3, \tag{1}$$

where I_x^i and I_z^i are, respectively, the x and z components of the spin-$1/2$ operator, ω_x and ω_z are the strengths of the transverse and longitudinal magnetic fields, respectively, and J_2 and J_3 are the Ising-type nearest-neighbor two-body and three-body coupling strengths, respectively. Here, the periodic boundary condition $I_z^{3+1} = I_z^1$ is used.

Figure 1 shows the schematic phase diagram of the ground state of the system and Table I identifies the ground states in the different areas. The competition between the three kinds of interactions (one-, two-, and three-body) results in different ground-state phases (product, W, and GHZ states). In regime I, the ground states are product states; in regime II, they are W-type states; and in regime III, they are GHZ-type states. The GHZ and W states are the only two inequivalent kinds of genuine tripartite entanglement in a three-spin system [21]. Whereas the W state can retain maximal expected bipartite entanglement when any one of the three spins is traced out, the GHZ state disentangles completely if a projective measurement is made on any spin. The GHZ states exist in region III, where the three-body interaction dominates.

TABLE I. Ground state for the Hamiltonian (1). Here $|\pm\rangle = (|0\rangle \pm |1\rangle)\sqrt{2}$, $|\text{GHZ}_\pm\rangle = (|000\rangle \pm |111\rangle)/\sqrt{2}$ and H is the Hadamard gate.

Region	Ground state
I	A: $\lvert 000\rangle$ B: $\lvert 111\rangle$ C: $\lvert{-}{-}{-}\rangle(\omega_x > 0)$ or $\lvert{+}{+}{+}\rangle(\omega_x < 0)$
II	A: $\lvert W_{001}\rangle = \frac{1}{\sqrt{3}}(\lvert 001\rangle + \lvert 010\rangle + \lvert 100\rangle)$ B: $\lvert W_{110}\rangle = \frac{1}{\sqrt{3}}(\lvert 110\rangle + \lvert 101\rangle + \lvert 011\rangle)$
III	A: $\lvert\overline{\text{GHZ}_+}\rangle = H^{\otimes 3}\lvert\text{GHZ}_+\rangle$ B: $\lvert\overline{\text{GHZ}_-}\rangle = H^{\otimes 3}\lvert\text{GHZ}_-\rangle$

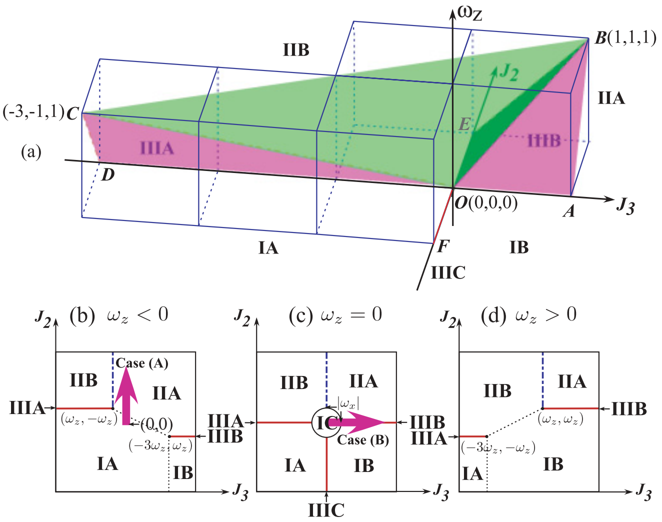

FIG. 1. (Color online) Schematic phase diagram of the ground state in a closed three-spin chain with the Hamiltonian of Eq. (1). (a) In three-dimensional parameter space ($J_3, J_2, \omega_z \geqslant 0$). W states and product states exist in the volumes separated by the three planes OAB, OBC, and OCD: inside for W states (region II) and in front for product states (region I). The GHZ states (region III) occupy only one-dimensional (phase IIIC on the ray from O through F) and two-dimensional regions (phase IIIA and IIIB on two half planes OAB and OCD). Panels (b), (c), and (d) show two-dimensional slices $\perp \omega_z$ for $\omega_z < 0$, $\omega_z = 0$, and $\omega_z > 0$, respectively. The arrows in (b) and (c) represent the adiabatic evolutions discussed in the experimental section. For (b) and (d), ω_x is assumed to be small (i.e., $|\omega_x| \ll |\omega_z|$).

In the following subsections, we separately consider two limiting cases in detail. In the first case, the qubits are coupled by pairwise interactions and in the second, we consider three-body interactions.

A. System with two-body interactions

We first consider a system consisting of spin-$1/2$ particles interacting by Ising-type nearest-neighbor couplings. For three spins, the system Hamiltonian is

$$\mathcal{H}_1 = \omega_z\left(I_z^1 + I_z^2 + I_z^3\right) + 2J_2\left(I_z^1 I_z^2 + I_z^2 I_z^3 + I_z^1 I_z^3\right). \tag{2}$$

If the sign of the coupling constant is positive, $J_2 > 0$, we obtain a quantum transition point at $\omega_z = 2J_2$. For a negative coupling constant, the ground state is always a product state and the system does not undergo a quantum transition. We therefore focus here on the antiferromagnetic case ($J_2 > 0$).

In the range $J_2 > |\omega_z|/2$, the ground state of this system is threefold degenerate. To avoid this complication, we add a small transverse magnetic field [19]. The resulting Hamiltonian is

$$\begin{aligned}\mathcal{H}_1' = {} & \omega_z\left(I_z^1 + I_z^2 + I_z^3\right) + \omega_x\left(I_x^1 + I_x^2 + I_x^3\right) \\ & + 2J_2\left(I_z^1 I_z^2 + I_z^2 I_z^3 + I_z^1 I_z^3\right).\end{aligned} \tag{3}$$

The transverse field will always be kept small, $|\omega_x| \ll |\omega_z|, |J_2|$.

Since the Hamiltonian is symmetric with respect to permutation of the qubits, we use a symmetry-adapted basis. The totally symmetric subspace is spanned by the states $|000\rangle$, $|W\rangle_{001}$, $|W\rangle_{110}$, and $|111\rangle$, where the W states are

$$|W\rangle_{001} = \frac{1}{\sqrt{3}}(|001\rangle + |010\rangle + |100\rangle),$$
$$|W\rangle_{110} = \frac{1}{\sqrt{3}}(|110\rangle + |101\rangle + |011\rangle). \tag{4}$$

In this subspace, the Hamiltonian has the matrix representation

$$\mathcal{H}'_{1s} = \frac{1}{2}\begin{pmatrix} 3\omega_z + 3J_2 & \sqrt{3}\omega_x & 0 & 0 \\ \sqrt{3}\omega_x & \omega_z - J_2 & 2\omega_x & 0 \\ 0 & 2\omega_x & -\omega_z - J_2 & \sqrt{3}\omega_x \\ 0 & 0 & \sqrt{3}\omega_x & -3\omega_z + 3J_2 \end{pmatrix}. \tag{5}$$

Within first-order perturbation theory, the ground state is

$$|\psi_g\rangle \approx \cos\frac{\theta_1}{2}|lll\rangle - \sin\frac{\theta_1}{2}|W\rangle_{ll\bar{l}},$$
$$\tan\theta_1 = \frac{\sqrt{3}\omega_x}{2(|\omega_z| - 2J_2)}. \tag{6}$$

If $\omega_z < 0$ then $|lll\rangle = |000\rangle$ and $|W\rangle_{ll\bar{l}} = |W\rangle_{001}$. If $\omega_z > 0$ then $|lll\rangle = |111\rangle$ and $|W\rangle_{ll\bar{l}} = |W\rangle_{110}$. If $J_2 > |\omega_z/2|$, the ground state contains a small contribution from the state $|W\rangle_{\bar{l}\bar{l}l}$ [of the order $\omega_x/\omega_z(\ll 1)$]. Figure 2(a) shows the energy-level diagram for this system for $\omega_z < 0$ as a function of the coupling strength J_2. Clearly, the character of the ground state changes qualitatively at the transition point $J_2 = |\omega_z/2|$:

$$|000\rangle \xrightarrow{J_2 = -\frac{1}{2}\omega_z} |W\rangle_{001}\ (\omega_z < 0),$$
$$|111\rangle \xrightarrow{J_2 = \frac{1}{2}\omega_z} |W\rangle_{110}\ \ (\omega_z > 0). \tag{7}$$

For weak coupling, the system ground state is a product state; for strong coupling (i.e., $J_2 > |\omega_z/2|$), it is an entangled state of all three spins.

B. Entanglement measures

In pure three-qubit systems, the two most commonly used entanglement measures are the two-tangle (i.e., concurrence) and the three-tangle [27]. The concurrence, which is related to the "entanglement of formation" [28], can be written as

$$\mathcal{C}_{ij} = \max\{\lambda_1 - \lambda_2 - \lambda_3 - \lambda_4, 0\},$$

where λ_α ($\alpha = 1, 2, 3, 4$) are the square roots of the eigenvalues of $\rho_{ij}(4I_y^i I_y^j)\rho_{ij}^*(4I_y^i I_y^j)$ in decreasing order and ρ_{ij} is the reduced density matrix for the two qubits i and j; $\rho_{ij} = \mathrm{Tr}_k(|\psi\rangle\langle\psi|)$, $(i \neq j \neq k)$, and $|\psi\rangle$ is the state of the full system. The concurrence measures the pairwise entanglement of a pair of qubits i and j. In the 3-qubit system, we use the average two-tangle τ_2 to quantify the average pairwise entanglement of all qubit pairs:

$$\tau_2 = \left(\mathcal{C}_{12}^2 + \mathcal{C}_{23}^2 + \mathcal{C}_{13}^2\right)/3.$$

The three-tangle τ_3 quantifies the essential three-way entanglement of a pure three-qubit state:

$$\tau_3 = \mathcal{C}_{i(jk)}^2 - \left(\mathcal{C}_{ij}^2 + \mathcal{C}_{ik}^2\right),$$

where the bipartite concurrence $\mathcal{C}_{i(jk)} = [2 - 2\mathrm{Tr}(\rho_i^2)]^{1/2}$ refers to the entanglement between qubit i and the pair jk [29,30].

In the system in Eq. (3), the ground state is an entangled state if the coupling strength exceeds the transition value $J_2 > |\omega_z/2|$. As shown in Fig. 2(b), the two-tangle τ_2 shows a transition at this point, changing from 0 to around 4/9 (the maximum value), while the three-tangle τ_3 remains close to zero throughout. In the limiting case ($\omega_x \to 0$), a W-entangled state can be generated by initializing the system into the ground state of the Hamiltonian (3) with weak coupling and adiabatically increasing the strength of the two-body interactions [31].

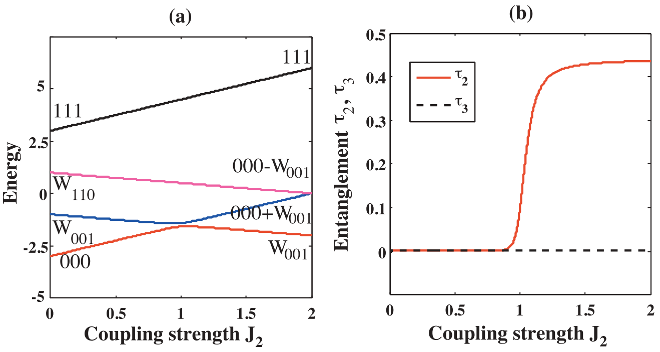

FIG. 2. (Color online) Energy-level diagram (a) and the ground-state entanglement (b), measured by the average two-tangle τ_2 and the three-tangle τ_3, for the Hamiltonian $\mathcal{H}'_{1s}$ [Eq. (5)] with $\omega_z = -2$ and $\omega_x = 0.1$.

C. System with three-body interactions

Different from the two-body interactions, an additional possible resource are three-body interactions [23], which exist in some real physical systems, for example in optical lattices constructed of equilateral triangles [22,32]. A rich variety of phases and critical points are found in spin chains with three-body interactions, such as incommensurate phases [33,34], chiral phase transitions [25,35], or quantum entanglement phase transitions [36,37]. Moreover, a speedup of quantum-state transfer is achieved through a Heisenberg spin chain with three-body interactions over that with two-body interactions [38].

The Hamiltonian with the three-body interaction that we consider is the simplest case, which is described by

$$\mathcal{H}_2 = \omega_x\left(I_x^1 + I_x^2 + I_x^3\right) + 4J_3 I_z^1 I_z^2 I_z^3. \tag{8}$$

For this system, the ground state is

$$|\psi_g\rangle \approx H^{\otimes 3}\left(\cos\frac{\theta_2}{2}|111\rangle - \sin\frac{\theta_2}{2}|000\rangle\right),$$
$$\tan\theta_2 = \frac{J_3}{3\omega_x}. \tag{9}$$

with the ground-state energy $E_g = -\frac{1}{2}[(3\omega_x)^2 + (J_3)^2]^{1/2}$, $\theta_2 \in [0, 2\pi)$ and the Hadamard gate

$$H = \frac{1}{\sqrt{2}}\begin{pmatrix} 1 & 1 \\ 1 & -1 \end{pmatrix}.$$

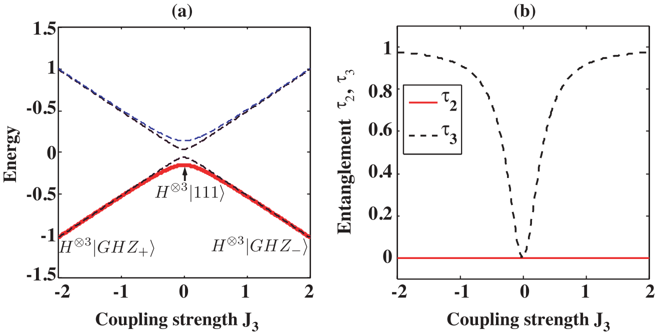

FIG. 3. (Color online) Energy-level diagram (a) and the ground-state entanglement (b), measured by the average two-tangle τ_2 and the three-tangle τ_3, for the Hamiltonian $\mathcal{H}_2$ [Eq. (8)] with $\omega_x = 0.1$.

Three most important limiting cases are

$$|\psi_g\rangle \approx \begin{cases} H^{\otimes 3}|\text{GHZ}\rangle_+, & J_3 \ll -|\omega_x| \\ H^{\otimes 3}|111\rangle, & J_3 = 0 \\ H^{\otimes 3}|\text{GHZ}\rangle_-, & J_3 \gg |\omega_x| \end{cases}, \tag{10}$$

where

$$|\text{GHZ}\rangle_\pm = \frac{1}{\sqrt{2}}(|000\rangle \pm |111\rangle). \tag{11}$$

Figure 3 shows the corresponding energy-level diagram and the ground-state entanglement. For strong coupling, $J_3 \gg |\omega_x|$, the ground state is now a three-way entangled state, as indicated by the limiting value for the three tangle, $\tau_3 \to 1$, while the two-tangle τ_2 vanishes for all coupling strengths. In the weak-coupling case, $J_3 \ll |\omega_x|$, the three tangle also vanishes, indicating that the system becomes a product state. The numerical simulations predict a critical point at $J_3 = \omega_x$ for the three-body Ising spin model in the thermodynamic limit [23–25,39–41]. Thus, genuine three-way entanglement (such as a GHZ state) can be generated by an adiabatic evolution of a Hamiltonian with a three-body interaction, such as the Hamiltonian (8).

We now consider the case of an additional uniform magnetic field along the z axis. The total Hamiltonian is then

$$\mathcal{H}_3 = \omega_z\left(I_z^1 + I_z^2 + I_z^3\right) + \omega_x\left(I_x^1 + I_x^2 + I_x^3\right) + 4J_3 I_z^1 I_z^2 I_z^3. \tag{12}$$

For the totally symmetric subspace considered above, the form of the Hamiltonian resembles that of the two-body interaction given in Eq. (3):

$$\mathcal{H}_3 = \frac{1}{2}\begin{pmatrix} 3\omega_z + J_3 & \sqrt{3}\omega_x & 0 & 0 \\ \sqrt{3}\omega_x & \omega_z - J_3 & 2\omega_x & 0 \\ 0 & 2\omega_x & -\omega_z + J_3 & \sqrt{3}\omega_x \\ 0 & 0 & \sqrt{3}\omega_x & -3\omega_z - J_3 \end{pmatrix}. \tag{13}$$

In zero-order perturbation theory, its ground state is

$$|\psi_g\rangle \approx \begin{cases} |111\rangle, & \omega_z > |\omega_x| \\ H^{\otimes 3}|\text{GHZ}\rangle_-, & \omega_z = 0 \\ |W\rangle_{001}, & -J_3 < \omega_z < 0 \\ |000\rangle, & \omega_z < -J_3. \end{cases} \tag{14}$$

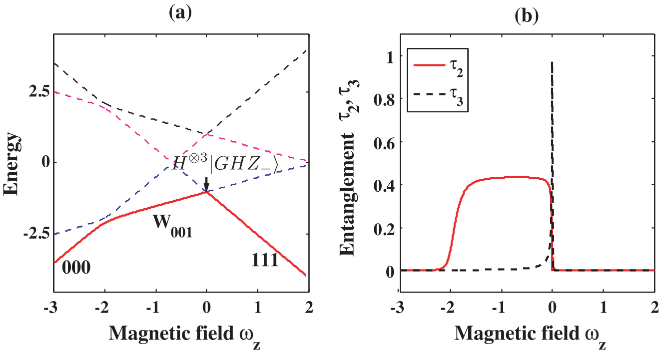

FIG. 4. (Color online) Energy-level diagram (a) and the ground-state entanglement (b), measured by the average two-tangle τ_2 and the three-tangle τ_3, for the Hamiltonian $\mathcal{H}_3$ [Eq. (12)] with $\omega_x = 0.1$ and $J_3 = 2$.

Equation (14) reveals a rich variety of ground states when $J_3 \gg |\omega_x|$. The corresponding energy-level diagram and the ground-state entanglement are plotted in Fig. 4, which shows that the introduction of a strong magnetic field changes the ground state from a GHZ state to a W state.

III. NMR IMPLEMENTATION

Our goal is to observe these quantum transitions in a real physical system and to quantify the entanglement in different phases. For this purpose, we chose a system of nuclear spins coupled by scalar exchange interactions. Using multiple pulse sequences, we generated effective Hamiltonians that correspond to the Hamiltonians (3) and (8) discussed in the previous section.

The three quantum spin-1/2 particles are represented by the ^{1}H, ^{19}F, and ^{13}C nuclear spins of Diethyl-fluoromalonate. The chemical structure of this molecule and the relevant parameters are shown in Fig. 5, where the three nuclei used as qubits are marked by the oval. We chose ^{13}C, ^{1}H, and ^{19}F as qubits 1, 2, and 3, respectively. Therefore, the natural Hamiltonian of the three-qubit system in the multiply rotating frame is

$$\mathcal{H}_{\text{NMR}} = \omega_0 \sum_{i=1}^{3} I_z^i + \sum_{i<j,=1}^{3} 2\pi J_{ij} I_z^i I_z^j, \tag{15}$$

where ω_0 is the effective static field in the rotating frame. It can be made identical for all three spins by suitably adjusting the transmitter's frequencies on all three channels. The main difference between this Hamiltonian and $\mathcal{H}_1$ is that the coupling constants in the natural Hamiltonian $\mathcal{H}_{\text{NMR}}$ are not identical. We therefore have to use a pulse sequence that "symmetrizes" the Hamiltonian.

Experiments were carried out at room temperature using a Bruker Avance II 500 MHz (11.7 T) spectrometer equipped with a QXI probe with pulsed field gradient. The middle figure in Fig. 5 shows the ^{13}C spectrum of the thermal state. The resonance of the ^{13}C spin is split into four transitions by the couplings to the ^{1}H and ^{19}F spins. In the figure, the labels near the transitions indicate the state of these passive spins.

The experiment, which is summarized in Fig. 6, includes three steps: we first initialize the system in the ground state of the uncoupled Hamiltonian ($J_2 = J_3 = 0$), where the ground

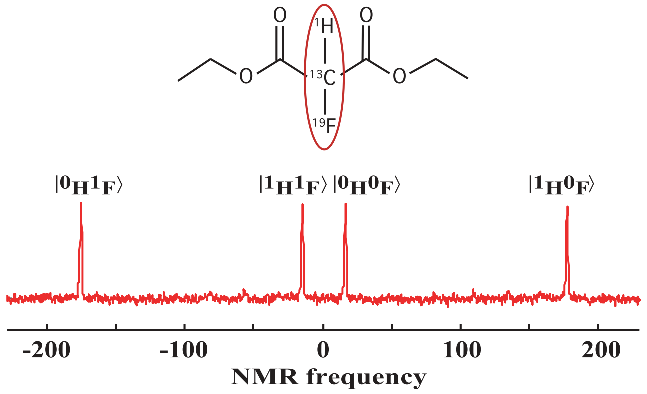

	^{13}C	^{1}H	^{19}F	T_1(s)	T_2(s)
^{13}C	125.79MHz			3.2	1.3
^{1}H	161.3Hz	500.23MHz		3.3	1.0
^{19}F	-192.2Hz	47.6Hz	470.59MHz	3.2	1.7

FIG. 5. (Color online) Relevant properties of the quantum register. The top part shows the molecular structure of Diethylfluoromalonate and the oval marks the three spins used as qubits. The central part shows the NMR spectrum of the ^{13}C obtained through a read-out $\pi/2$ pulse on the equilibrium state, where the four resonance lines are labeled by the corresponding states of the two other qubits. The table at the bottom summarizes the relevant NMR parameters; that is, the resonance frequencies ω_i (on the diagonal), the J-coupling constants J_{ij} (below the diagonal), and the relaxation times T_1 and T_2 in the last two columns.

state is a product state. We then change the Hamiltonian adiabatically to generate an adiabatic evolution of the system through a transition point. At different steps along this trajectory, we measure the two- and three-spin correlations. At the start and end points, we also perform a complete density-operator tomography [19].

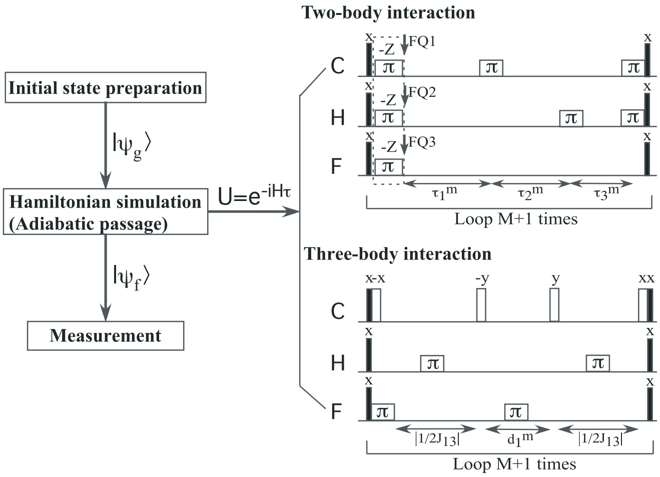

FIG. 6. General scheme for observing the variation of the ground state of a quantum system (left-hand side) and the pulse sequences (right-hand side) for simulating the Hamiltonians with two-body interaction Eq. (3) (top part) and three-body interaction Eq. (8) (bottom part). The narrow black rectangles represent small-angle rotations, whereas the narrow empty rectangles denote 90° rotations and the wide ones denote the refocusing 180° pulses. The delays are $\tau_1^m = 2J_2(m)\tau/[1/(\pi J_{12}) + 1/(\pi J_{23})]$, $\tau_2^m = 2J_2(m)\tau/[1/(\pi J_{23}) + 1/(\pi|J_{13}|)]$, $\tau_3^m = 2J_2(m)\tau/[1/(\pi J_{12}) + 1/(\pi|J_{13}|)]$, and $d_1^m = 4J_3(m)\tau/(\pi J_{12})$.

A. Initial state preparation

We initialized the system in the ground state of the initial Hamiltonian by preparing a pseudopure state (PPS) $\rho_{000} = (1-\epsilon)\mathbf{1}/8 + \epsilon|000\rangle\langle000|$ using spatial averaging techniques [42]. Here $\mathbf{1}$ represents the unity operator and $\epsilon \approx 10^{-5}$ represents the thermal polarization. The $|0\rangle$ and $|1\rangle$ states correspond to the two eigenstates of I_z—the spin-up and spin-down states, respectively. The density matrix of the PPS, ρ_{000}, was reconstructed using quantum state tomography [43,44], which involves the application of 7 readout pulses and recording of the spectra of all three channels to obtain the coefficients for the 64 operators comprising a complete operator basis of the three-spin system. As an example, Fig. 7(a) shows the experimental spectrum obtained after applying a $(\pi/2)_y$ readout pulse to the carbon spin for the prepared PPS. Because we used an unlabeled sample, the ^{1}H and ^{19}F spectra were dominated by signals from molecules with the ^{12}C isotope, while the signals from the quantum register with the ^{13}C nucleus appeared only as small ($\approx$0.5%) satellites. To effectively separate this signal from that of the dominant background, we employed a SWAP gate to transfer the state of the ^{1}H or ^{19}F qubit to the ^{13}C qubit and read the state through the ^{13}C spectrum. The measured transfer efficiency was 0.98 for ^{1}H and 0.90 for ^{19}F. These factors were taken into account for the reconstruction of the density operator

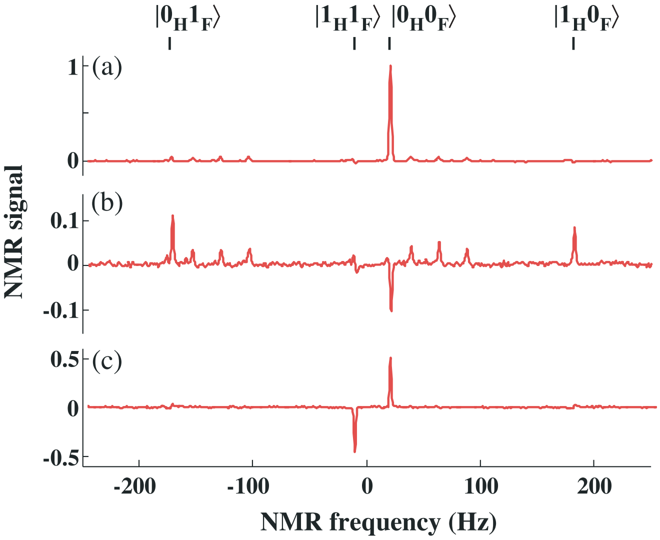

FIG. 7. (Color online) ^{13}C experimental spectra after a $(\pi/2)_y$ readout pulse was applied to the carbon for (a) the pseudopure state ρ_{000}, (b) the W state corresponding to the ground state of the Hamiltonian (3) with $J_2 = 2$, and (c) the GHZ state corresponding to the ground state of the Hamiltonian (8) with $J_3 = 2$. The additional lines in spectrum (b) can be assigned to molecules in which the ^{1}H spins were exchanged with ^{2}H spins from the solvent. These additional lines did not contribute to the result, since we only measured the amplitudes of the resonance lines from the protonated molecules.

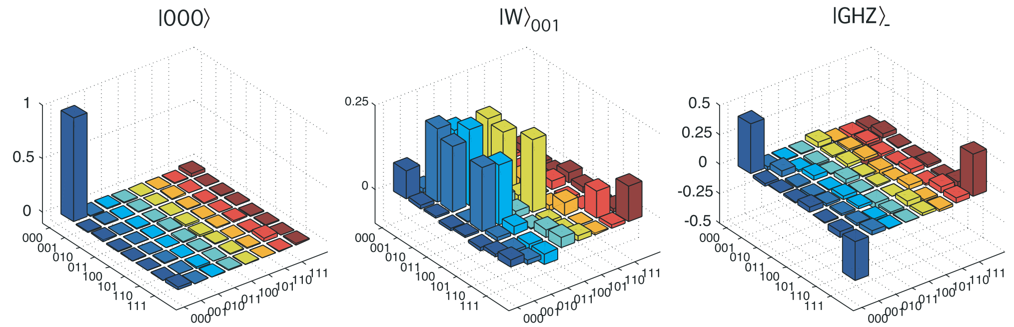

FIG. 8. (Color online) Real part of the density matrices for the initial state $|000\rangle$ (left part), the W state (middle part) corresponding to the ground state of Hamiltonian (3) with strong coupling, and the GHZ state (right part) corresponding to the ground state of Hamiltonian (8) with strong coupling. The rows and columns represent the standard computational basis in binary order, from $|000\rangle$ to $|111\rangle$.

$\rho_{\text{expt}} \equiv [\rho - (1-\epsilon)\mathbf{1}/8]/\epsilon$. The leftmost plot in Fig. 8 shows the measured density operator for the initial pseudopure state. Its experimentally determined state fidelity was

$$F(\rho_{\text{theor}}, \rho_{\text{expt}}) = \frac{\text{Tr}(\rho_{\text{theor}}\rho_{\text{expt}})}{\sqrt{\text{Tr}(\rho_{\text{theor}}^2)\text{Tr}(\rho_{\text{expt}}^2)}} \approx 0.99. \qquad (16)$$

The ground state of the initial Hamiltonian $\mathcal{H}_1(0)$ [Eq. (3)] with $\omega_z = -2$ and $J_2(0) = 0$ is close to $|000\rangle$, which we prepared as a PPS. In the case of the three-body Hamiltonian [Eq. (8)], the ground state of $\mathcal{H}_2(0)$ with $J_3(0) = 0$ is $(1/\sqrt{8})(|0\rangle - |1\rangle)^{\otimes 3}$. This state was prepared by applying $\pi/2$ pulses along the $-y$ axis to each qubit of the state ρ_{000}.

B. Hamiltonian simulation

The target Hamiltonian can be created as an average Hamiltonian by concatenating evolutions with short periods:

$$\begin{aligned} e^{-i\mathcal{H}_{\text{tar}}\tau} &= e^{-i(\mathcal{H}_x+\mathcal{H}_z)\tau} \\ &= e^{-i\mathcal{H}_x\tau/2}e^{-i\mathcal{H}_z\tau}e^{-i\mathcal{H}_x\tau/2} + O(\tau^3), \end{aligned} \qquad (17)$$

where

$$\mathcal{H}_x = \omega_x\left(I_x^1 + I_x^2 + I_x^3\right)$$

and $\mathcal{H}_z$ is either $2J_2(I_z^1 I_z^2 + I_z^2 I_z^3 + I_z^1 I_z^3) + \omega_z(I_z^1 + I_z^2 + I_z^3)$ for Hamiltonian $\mathcal{H}_1'$ of Eq. (3) or $4J_3 I_z^1 I_z^2 I_z^3$ for Hamiltonian $\mathcal{H}_2$ of Eq. (8). The approximation is valid as long as the evolution period τ is kept sufficiently short. Here and in the following, we will use dimensionless units for the parameters J_2 and J_3 of the target Hamiltonian and the associated evolution times τ and T.

The adiabatic passage requires a time-dependent Hamiltonian. To ensure that the system always stays in the instantaneous ground sate, the variation of the control parameter J has to be sufficiently slow, so that the adiabatic condition [45]

$$\left|\frac{\langle\psi_{\text{g}}(t)|\dot{\psi}_{\text{e}}(t)\rangle}{\varepsilon_{\text{e}}(t) - \varepsilon_{\text{g}}(t)}\right| \ll 1$$

is fulfilled, where $|\psi_{\text{g}}(t)\rangle$ and $|\psi_{\text{e}}(t)\rangle$ refer to the instantaneous ground state and the first excited state, respectively, and $\varepsilon_{\text{g}}(t)$ and $\varepsilon_{\text{e}}(t)$ are the corresponding energies.

For the experimental realization, we implemented the variation as a sequence of $M+1$ time-invariant Hamiltonians

$$\mathcal{H}(m) = \mathcal{H}\left(J\left(\frac{m}{M}T\right)\right),$$

where T is the total duration of the adiabatic passage and $m = 0$ to M. The duration of each step is $\tau = T/(M+1)$. Together with the total number of steps $M+1$, it has to fulfill two conditions: (i) the time τ must be short enough that the average Hamiltonian approximation (17) holds and (ii) the adiabaticity criterion remains valid. Considering the splitting of the energy levels during the scan, it is clear that a linear interpolation is not a good solution. Instead, we used a hyperbolic sine for the variation of the control parameters J_2 and J_3 [19,26].

1. *Two-body interaction*

All the pairwise couplings between the qubits in the molecule have nonzero strength. However, they are not identical. We therefore have to modify the natural Hamiltonian, using an appropriate pulse sequence. We therefore used a refocusing scheme [46–48] that also takes the negative sign of the coupling constant J_{13} into account.

The top figure on the right side of Fig. 6 shows the pulse sequence that we used for the simulation of the Hamiltonian $\mathcal{H}_1$. We generated the appropriate frequency offset ω_z of Eq. (4) by setting the transmitter's frequency of each channel to the appropriate value (FQn in Fig. 6). For the adiabatic scan, we incremented the coupling constant J_2 from 0 to 2 in 9 segments ($M = 8$) and set the duration τ of each segment to $\pi/2$. The longitudinal field of Eq. (4) was set to $\omega_z = -2$, the transverse field to $\omega_x = 0.19$. For the segment m, the radio-frequency offsets for three channels are set as $\text{FQ1}^m = -\pi/(\tau_1^m - \tau_2^m + 3\tau_3^m)$, $\text{FQ2}^m = -\pi/(\tau_1^m + \tau_2^m - \tau_3^m)$, and $\text{FQ3}^m = -\pi/(\tau_1^m + \tau_2^m + \tau_3^m)$.

2. *Three-body interaction*

In NMR, nature does not provide three-body interactions between nuclear spins, but they can be simulated by a combination of two-body interactions and radio-frequency pulses [49]:

$$\begin{aligned} U_{zzz} &= e^{-i4J_3 I_z^1 I_z^2 I_z^3 \tau} \\ &= e^{-i\frac{\pi}{4}I_x^1}e^{-i\pi I_z^1 I_z^3}e^{-i\frac{\pi}{4}I_y^1}e^{-i2J_3 I_z^1 I_z^2\tau}e^{i\frac{\pi}{4}I_y^1}e^{i\pi I_z^1 I_z^3}e^{i\frac{\pi}{4}I_x^1}. \end{aligned} \qquad (18)$$

To implement this, we use the relation

$$e^{i\pi I_z^i I_z^j} = e^{i\pi I_x^i} e^{-i\pi I_z^i I_z^j} e^{i\pi I_x^i}.$$

The pulse sequence that generates the Hamiltonian (8) is shown in the bottom part of the right-hand side of Fig. 6. Experiments were performed using $\tau = \pi/2$, $M = 8$, $J_3(0) = 0$, $J_3(T) = 2$, and $\omega_x = 0.12$.

C. Readout

To distinguish the different phases and measure the corresponding entanglement(s), we performed a complete density operator tomography of the initial and final states, corresponding to $J_2(0)$ and $J_2(T)$ [and $J_3(0)$ and $J_3(T)$, respectively]. The reconstruction procedure included the measurement of a total of 21 spectra, extraction of the amplitudes and phases of the four resonance lines in each spectrum, and a fit of the density operator components to these values.

Figure 7 shows the ^{13}C experimental spectra obtained after applying a $(\pi/2)_y$ readout pulse to the carbon on the final state after the adiabatic evolution under Hamiltonian $\mathcal{H}_1'$ (b) and Hamiltonian $\mathcal{H}_2$ (c). Figure 8 shows the real parts of the reconstructed density matrices corresponding to the initial state $|000\rangle$ and the two final states $|W\rangle_{001}$ and $|\mathrm{GHZ}\rangle_-$. Rather than presenting the real ground state of Hamiltonian $\mathcal{H}_2$, we show its Hadamard transform, the GHZ state, whose density operator has a cleaner signature. For this purpose, we applied three $(\pi/2)_y$ pulses to the three qubits before the actual readout and reconstruction procedure. The initial state and the GHZ state are very close to the corresponding theoretical states, whereas the deviations between experiment and theory are somewhat larger for the W state. These results clearly show that the adiabatic evolution under the Hamiltonian (3) with two-body interactions creates a W state, which contains only pairwise entanglement among three spins, whereas the corresponding evolution under the three-body Hamiltonian (8) creates a GHZ state, which contains genuine three-way entanglement.

We used two different measures to compare the experimental and theoretical values of the final states: First, we consider the attenuated correlation [50]

$$c(\rho_{\mathrm{expt}}) = \frac{\mathrm{Tr}(\rho_{\mathrm{theor}}\rho_{\mathrm{expt}})}{\mathrm{Tr}(\rho_{\mathrm{theor}}\rho_{\mathrm{theor}})}, \tag{19}$$

where ρ_{theor} is a theoretical output state, obtained by applying the ideal transformations to the experimental input state $\rho_{000}^{\mathrm{expt}}$, and ρ_{expt} is the experimental output state obtained by density operator tomography. Equation (19) implies that $-1 \leqslant c \leqslant 1$. The experimental values of the correlation for the two cases considered here were $c(\rho_{\mathrm{expt}}^{W}) = 0.61$ and $c(\rho_{\mathrm{expt}}^{\mathrm{GHZ}}) = 0.73$. As the second measure, we removed the effect of spin relaxation from the measured final states by calculating the experimental fidelity (16), which yielded $F(\rho_{\mathrm{expt}}^{W}) = 0.90$ and $F(\rho_{\mathrm{expt}}^{\mathrm{GHZ}}) = 0.92$.

We also monitored the state of the system during the scan. Since a complete density operator tomography after every step would involve a very large number of measurements, we used two simpler measures: the average two-body correlation $C_2 = \sum_{i\neq j}\langle 4I_x^i I_x^j\rangle/3$ and the three-body correlation $C_3 = \langle 8I_x^1 I_x^2 I_x^3\rangle$. Figure 9 shows the result of these measurements.

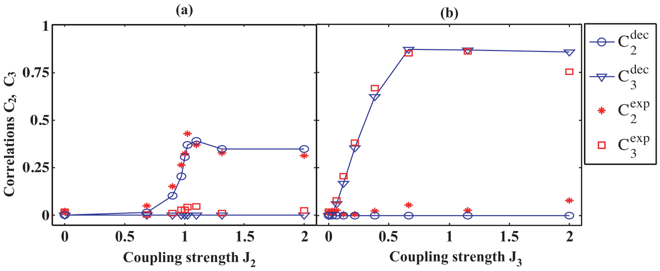

FIG. 9. (Color online) Multispin correlations indicating the change of the ground state at the transition point for the system (a) with two-body interaction $\mathcal{H}_1'$ for $\omega_z = -2$ and $\omega_x = 0.09$ and (b) with three-body interaction $\mathcal{H}_2$ for $\omega_x = 0.12$. The points indicate the average two-spin correlation and three-spin correlation obtained from the experiment [C_2^{exp} ($*$) and C_3^{exp} ($\square$)], and from a simulation of the adiabatic transfer procedure [C_2^{dec} ($\bigcirc$) and C_3^{dec} ($\triangledown$)].

As expected, the system of Hamiltonian (3) shows the generation of two-body correlation C_2 and almost no three-body correlation C_3 after the transition point at $J_2 = 1$, whereas the system of Hamiltonian (8) shows the transition by a large change in C_3 and almost no change in C_2.

The experimentally determined correlations are generally smaller than the theoretical values. This deviation can be attributed to decoherence. To verify this, we simulated the experiments by using the decoherence model of Ref. [51]. We obtained good agreement between theoretical and experimental data if we assumed an average decoherence time of 150 ms for system (3) and 600 ms for system (8). In system (8), the symmetric pulse sequence eliminated the inhomogeneity of the static magnetic field to some extent. The run time of the experiments was about 146 ms for system (3) and 62 ms for system (8). The simulated values are also shown in Fig. 9 as circles and triangles.

IV. ENTANGLEMENT AND QUANTUM PHASE TRANSITION

Recently, many researchers have studied aspects of entanglement properties of the ground state in the vicinity of quantum phase transitions, such as the scaling behavior of different entanglement measures [5–13]. The most frequently used entanglement measure is the two-qubit concurrence. However, it has been shown that a single type of concurrence is not sufficient to characterize all types of QPTs [22]. For example, in the three-spin system described by Eq. (8), the two-qubit concurrence of the ground state is always zero, since the entangled ground state is a GHZ state, which has no pairwise entanglement. More generally, the ground-state concurrence is not a good parameter for characterizing QPTs in systems that involve multipartite interactions [22,25,37].

It is thus important to consider alternative measures of entanglement. In our earlier study of complementarity [52], we conjectured that the local bipartite concurrence C_k between qubit k and the remaining system consisting of $N-1$ qubits,

$$\mathcal{C}_k = \sqrt{2\left[1 - \mathrm{Tr}\left(\rho_k^2\right)\right]}, \tag{20}$$

depends on all orders m of the entanglement of qubit k: $\mathcal{C}_k^2 = \sum_{m=2}^{N} \tau_m^{(k)}$. Therefore, the average (over all qubits) local

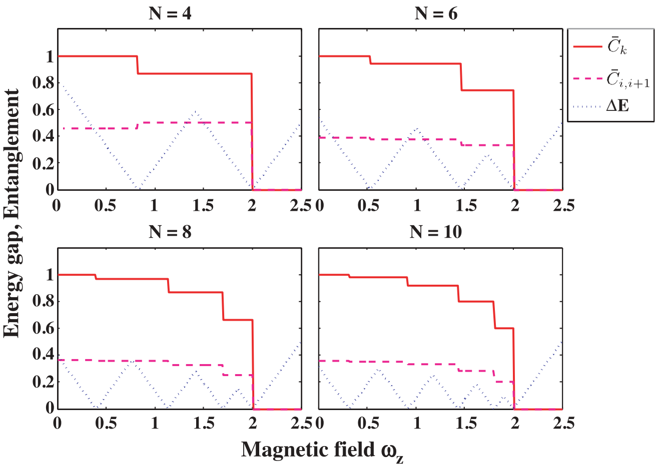

FIG. 10. (Color online) Numerical simulation of the average local concurrence $\bar{\mathcal{C}}_k$, the nearest-spin concurrence $\bar{\mathcal{C}}^{(i,i+1)}$, and the energy gap $\Delta E = E_{\mathrm{ex}} - E_{\mathrm{g}}$ between the ground state and the first excited state for the finite-size Heisenberg XX spin model on the circle consisting of an even number of spins. Here, $J = 1$ is assumed.

concurrence, $\bar{\mathcal{C}}_k = \sum_{k=1}^{N} \mathcal{C}_k/N$, may be used as an order parameter for describing the entanglement in QPTs.

As an example, we consider a finite-size Heisenberg XX model on the circle in a uniform external magnetic field:

$$H_{XX} = -\omega_z \sum_{i}^{N} I_z^i - 2J \sum_{i}^{N} \left(I_x^i I_x^{i+1} + I_y^i I_y^{i+1}\right),$$

with the periodic boundary conditions $I_\alpha^{N+1} = I_\alpha^1$, ($\alpha = x,y,z$). This Hamiltonian can be diagonalized by a Jordan-Wigner transformation followed by a deformed Fourier transform [53]. The spectrum, in particular its ground-state energy and the ground state have been discussed in [53,54]. They also showed that the thermodynamical limit is very rapidly approached, so that a 10-qubit system already represents a very good approximation [53].

We now consider the different entanglement measures of the ground state as a function of the external magnetic field strength. Figure 10 plots them for the even values of N and Fig. 11 for the odd values. We compare the average local concurrence $\bar{\mathcal{C}}_k$ to the average nearest-neighbor concurrence $\bar{\mathcal{C}}^{(i,i+1)} = \sum_i \mathcal{C}_{i,i+1}/N$. The graphs also show the energy difference between the ground state and the first excited state. Only positive magnetic fields are shown, the curves for negative field values are identical. It can be seen from these plots that the entanglement measures of both $\bar{\mathcal{C}}^{(i,i+1)}$ and $\bar{\mathcal{C}}_k$ are not continuous: the sudden changes at the energy level crossing points ($\Delta E = 0$). The jumps of $\bar{\mathcal{C}}_k$ are more pronounced than those of $\bar{\mathcal{C}}^{(i,i+1)}$, which illustrates that the ground state changes qualitatively at the points of degeneracy. In particular, for $|\omega_z| > 2$, the ground state of the model is a completely separable state (i.e., no entanglement), whereas for the region close to $|\omega_z| = 0$, the maximal entanglement is reached. For even N, the average local concurrence $\bar{\mathcal{C}}_k = 1$ (the maximally entangled state) and for odd N $\bar{\mathcal{C}}_k \to 1$ as N increases. For all N, the discontinuity of the entanglement measures is largest at $|\omega_z| = 2$, and its size decreases with increasing N.

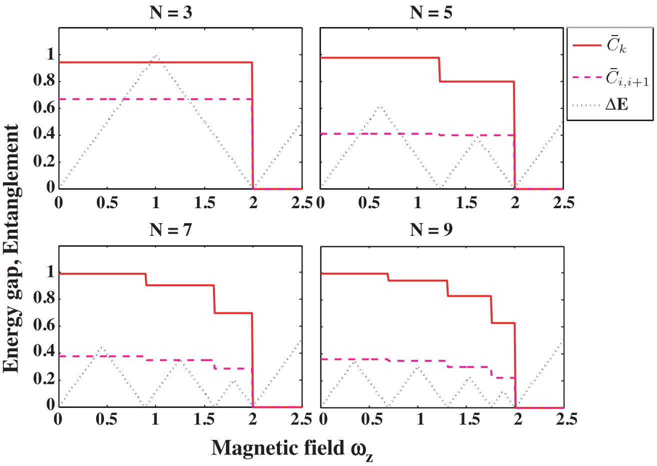

FIG. 11. (Color online) Numerical simulation of the average local concurrence $\bar{\mathcal{C}}_k$, the nearest-spin concurrence $\bar{\mathcal{C}}^{(i,i+1)}$, and the energy gap $\Delta E = E_{\mathrm{ex}} - E_{\mathrm{g}}$ between the ground state and the first excited state for the finite-size Heisenberg XX spin model on the circle consisting of an odd number of spins. Here, $J = 1$ is assumed.

The average local concurrence $\bar{\mathcal{C}}_k$ decreases monotonically with increasing field, with clearly noticeable steps. However, the average nearest-neighbor concurrence $\bar{\mathcal{C}}^{(i,i+1)}$ changes only very slightly at some level crossings and, for $N = 4$, the curve is not monotonic, and its maximum value is irregular. This is related to the fact that $\bar{\mathcal{C}}^{(i,i+1)}$ does not contain information on the features of multispin entanglement whereas $\bar{\mathcal{C}}_k$ does [52]. For large N, entanglement tends to be well distributed among all the spins in various forms. Therefore the average local concurrence $\bar{\mathcal{C}}_k$ is the more useful indicator of QPTs in the thermodynamic limit.

V. CONCLUSION

In conclusion, we have provided an experimental investigation of quantum transitions in a three-spin system with two- or three-body interactions, involving different types of entanglement. Depending on the control parameter, the ground state of the system is either a product state or an entangled state. If it is entangled, it can be either a W state (corresponding to pairwise entanglement without genuine three-way entanglement), or a GHZ state (genuine three-way entanglement without pairwise entanglement), depending on the type of interaction among three spins.

Using an NMR quantum simulator, we have experimentally confirmed that in this system the ground state undergoes a quantum transition from a product state to multipartite entangled states (W state or GHZ state) if the strength of the coupling between the spins becomes bigger than the Zeeman interaction. If the coupling consists only of pairwise interactions, the resulting state is a W state. In this case, the level crossing leads to a first-order phase transition of the ground state from a paramagnetic state in the weak-coupling case to an antiferromagnetically ordered state in the strong-coupling case. If it consists of three-body interactions, the ground state is a GHZ state. For this three-body Ising spin model, there exists a quantum transition which can be predicted at $J_3 = \omega_x$ in the thermodynamic limit [22–25,39–41]. Adiabatically changing the Hamiltonian through the different kinds of transitions, we have demonstrated how the different multipartite entangled states can be generated by tuning a single parameter. For the characterization of the quantum transitions, we used quantum state tomography of the initial and final state. During the scan, we measured the average two-spin and three-spin correlations, which proved to be useful order parameters for the model systems considered here.

Due to the complexity of the entanglement in multiqubit systems [52], it is difficult to characterize the transition of the ground-state entanglement in multiqubit systems. The next larger system, consisting of four qubits, can be entangled in nine different ways [55]. Most of the previous work used the nearest-neighbor pairwise entanglement $\mathcal{C}_{i,i+1}$ (i.e., concurrence) [5,16,17,56–60] or entanglement entropy [6,9,61–65]. As we and others have shown, these measures are not always suitable and should be considered incomplete. Numerical simulations of simple systems with larger numbers of qubits indicate that the average local entanglement $\bar{\mathcal{C}}_k$ may be a more general measure for the characterization of entangling QPTs.

ACKNOWLEDGMENTS

This work is supported by the CAS, NNSFC (under Grants No. 10975124 and No. 10674123), NFRP (under Grant No. 2007CB925200), and the DFG through Su 192/19-1. J. F. Zhang is currently at the University of Waterloo, Waterloo, Canada.

[1] S. Sachdev, *Quantum Phase Transition* (Cambridge University Press, Cambrige, 1999).

[2] F. Gebbhard, *The Mott Metal Insulator Transition: Models and Methods* (Springer-Verlag, New York, 1997).

[3] M. Greiner, O. Mandel, T. Esslinger, T. W. Hänsch, and I. Bloch, Nature (London) **415**, 39 (2002).

[4] R. B. Laughlin, Phys. Rev. Lett. **50**, 1395 (1983).

[5] A. Osterloh, L. Amico, G. Falci, and R. Fazio, Nature (London) **416**, 608 (2002).

[6] G. Vidal, J. I. Latorre, E. Rico, and A. Kitaev, Phys. Rev. Lett. **90**, 227902 (2003).

[7] J. Vidal, G. Palacios, and R. Mosseri, Phys. Rev. A **69**, 022107 (2004).

[8] T. J. Osborne and M. A. Nielsen, Phys. Rev. A **66**, 032110 (2002).

[9] J. Latorre, E. Rico, and G. Vidal, Quantum Inf. Comput. **4**, 48 (2002).

[10] F. Verstraete, M. Popp, and J. I. Cirac, Phys. Rev. Lett. **92**, 027901 (2004).

[11] S.-J. Gu, S.-S. Deng, Y.-Q. Li, and H.-Q. Lin, Phys. Rev. Lett. **93**, 086402 (2004).

[12] A. Anfossi, P. Giorda, and A. Montorsi, Phys. Rev. B **75**, 165106 (2007).

[13] D. Larsson and H. Johannesson, Phys. Rev. Lett. **95**, 196406 (2005).

[14] L. Zhou, H. S. Song, Y. Q. Guo, and C. Li, Phys. Rev. A **68**, 024301 (2003).

[15] X. Wang, Phys. Rev. A **66**, 034302 (2002).

[16] G. Lagmago Kamta and A. F. Starace, Phys. Rev. Lett. **88**, 107901 (2002).

[17] M. C. Arnesen, S. Bose, and V. Vedral, Phys. Rev. Lett. **87**, 017901 (2001).

[18] A. Friedenauer, H. Schmitz, J. T. Gluechert, D. Porras, and T. Schaetz, Nature Phys. **4**, 757 (2008).

[19] X. Peng, J. Du, and D. Suter, Phys. Rev. A **71**, 012307 (2005).

[20] J. Zhang, X. Peng, N. Rajendran, and D. Suter, Phys. Rev. Lett. **100**, 100501 (2008).

[21] W. Dür, G. Vidal, and J. I. Cirac, Phys. Rev. A **62**, 062314 (2000).

[22] J. K. Pachos and M. B. Plenio, Phys. Rev. Lett. **93**, 056402 (2004).

[23] R. J. Baxter and F. Y. Wu, Phys. Rev. Lett. **31**, 1294 (1973).

[24] F. Igloi, D. V. Kapor, M. Skrinjar, and J. Solyom, J. Phys. A **16**, 4067 (1983).

[25] C. D'Cruz and J. K. Pachos, Phys. Rev. A **72**, 043608 (2005).

[26] X. Peng, J. Zhang, J. Du, and D. Suter, Phys. Rev. Lett. **103**, 140501 (2009).

[27] V. Coffman, J. Kundu, and W. K. Wootters, Phys. Rev. A **61**, 052306 (2000).

[28] W. K. Wootters, Phys. Rev. Lett. **80**, 2245 (1998).

[29] P. Rungta, V. Bužek, C. M. Caves, M. Hillery, and G. J. Milburn, Phys. Rev. A **64**, 042315 (2001).

[30] P. Rungta and C. M. Caves, Phys. Rev. A **67**, 012307 (2003).

[31] N. F. Bell, R. F. Sawyer, R. R. Volkas, and Y. Y. Y. Wong, Phys. Rev. A **65**, 042328 (2002).

[32] J. K. Pachos and E. Rico, Phys. Rev. A **70**, 053620 (2004).

[33] H. Frahm, J. Phys. A **25**, 1417 (1992).

[34] A. M. Tsvelik, Phys. Rev. B **42**, 779 (1990).

[35] D. I. Tsomokos, J. J. García-Ripoll, N. R. Cooper, and J. K. Pachos, Phys. Rev. A **77**, 012106 (2008).

[36] P. Lou, W.-C. Wu, and M.-C. Chang, Phys. Rev. B **70**, 064405 (2004).

[37] M.-F. Yang, Phys. Rev. A **71**, 030302 (2005).

[38] J. Zhang, X. Peng, and D. Suter, Phys. Rev. A **73**, 062325 (2006).

[39] K. A. Penson, R. Jullien, and P. Pfeuty, Phys. Rev. B **26**, 6334 (1982).

[40] K. A. Penson, J. M. Debierre, and L. Turban, Phys. Rev. B **37**, 7884 (1988).

[41] F. Igloi, J. Phys. A **20**, 5319 (1987).

[42] D. G. Cory, M. D. Price, and T. F. Havel, Physica D **120**, 82 (1998).

[43] I. L. Chuang, N. Gershenfeld., M. G. Kubinec, and D. W. Leung, Proc. R. Soc. London, Sect. A **454**, 447 (1998).

[44] G. M. Leskowitz and L. J. Mueller, Phys. Rev. A **69**, 052302 (2004).

[45] A. Messiah, *Quantum Mechanics* (Wiley, New York, 1976).

[46] N. Linden, B. Herve, R. J. Carbajo, and R. Freeman, Chem. Phys. Lett. **305**, 28 (1999).

[47] N. Linden, E. Kupce, and R. Freeman, Chem. Phys. Lett. **311**, 321 (1999).

[48] J. A. Jones and E. Knill, J. Magn. Reson. **141**, 322 (1999).

[49] C. H. Tseng, S. Somaroo, Y. Sharf, E. Knill, R. Laflamme, T. F. Havel, and D. G. Cory, Phys. Rev. A **61**, 012302 (1999).

[50] G. Teklemariam, E. M. Fortunato, M. A. Pravia, T. F. Havel, and D. G. Cory, Phys. Rev. Lett. **86**, 5845 (2001).

[51] L. M. K. Vandersypen, M. Steffen, G. Breyta, C. S. Yannoni, M. H. Sherwood, and I. L. Chuang, Nature (London) **414**, 883 (2001).

[52] X. Peng, X. Zhu, D. Suter, J. Du, M. Liu, and K. Gao, Phys. Rev. A **72**, 052109 (2005).

[53] A. De Pasquale, G. Costantini, P. Facchi, G. Florio, S. Pascazio, and K. Yuasa, Eur. Phys. J. Special Topics **160**, 127 (2008).

[54] A. D. Pasquale and P. Facchi, Phys. Rev. A **80**, 032102 (2009).

[55] F. Verstraete, J. Dehaene, B. De Moor, and H. Verschelde, Phys. Rev. A **65**, 052112 (2002).

[56] O. Osenda, Z. Huang, and S. Kais, Phys. Rev. A **67**, 062321 (2003).

[57] Z.-Y. Sun, K.-L. Yao, W. Yao, D.-H. Zhang, and Z.-L. Liu, Phys. Rev. B **77**, 014416 (2008).

[58] V. Subrahmanyam, Phys. Rev. A **69**, 022311 (2004).

[59] F. C. Alcaraz, A. Saguia, and M. S. Sarandy, Phys. Rev. A **70**, 032333 (2004).

[60] X. Wang, Phys. Rev. A **64**, 012313 (2001).

[61] J. Zhao, I. Peschel, and X. Wang, Phys. Rev. B **73**, 024417 (2006).

[62] A. Kopp and K. Le Hur, Phys. Rev. Lett. **98**, 220401 (2007).

[63] X. Jia, A. R. Subramaniam, I. A. Gruzberg, and S. Chakravarty, Phys. Rev. B **77**, 014208 (2008).

[64] L. Cincio, J. Dziarmaga, M. M. Rams, and W. H. Zurek, Phys. Rev. A **75**, 052321 (2007).

[65] C. Wellard and R. Orús, Phys. Rev. A **70**, 062318 (2004).